

1 Improvement in Fast Particle Track Reconstruction  
2 with Robust Statistics

3 M. G. Aartsen<sup>2</sup>, R. Abbasi<sup>27</sup>, Y. Abdou<sup>22</sup>, M. Ackermann<sup>41</sup>, J. Adams<sup>15</sup>,  
4 J. A. Aguilar<sup>21</sup>, M. Ahlers<sup>27</sup>, D. Altmann<sup>9</sup>, J. Auffenberg<sup>27</sup>, X. Bai<sup>31,1</sup>,  
5 M. Baker<sup>27</sup>, S. W. Barwick<sup>23</sup>, V. Baum<sup>28</sup>, R. Bay<sup>7</sup>, J. J. Beatty<sup>17,18</sup>,  
6 S. Bechet<sup>12</sup>, J. Becker Tjus<sup>10</sup>, K.-H. Becker<sup>40</sup>, M. Bell<sup>38</sup>,  
7 M. L. Benabderrahmane<sup>41</sup>, S. BenZvi<sup>27</sup>, J. Berdermann<sup>41</sup>, P. Berghaus<sup>41</sup>,  
8 D. Berley<sup>16</sup>, E. Bernardini<sup>41</sup>, A. Bernhard<sup>30</sup>, D. Bertrand<sup>12</sup>, D. Z. Besson<sup>25</sup>,  
9 G. Binder<sup>8,7</sup>, D. Bindig<sup>40</sup>, M. Bissok<sup>1</sup>, E. Blaufuss<sup>16</sup>, J. Blumenthal<sup>1</sup>,  
10 D. J. Boersma<sup>39</sup>, S. Bohaichuk<sup>20</sup>, C. Bohm<sup>34</sup>, D. Bose<sup>13</sup>, S. Böser<sup>11</sup>,  
11 O. Botner<sup>39</sup>, L. Brayeur<sup>13</sup>, H.-P. Bretz<sup>41</sup>, A. M. Brown<sup>15</sup>, R. Bruijn<sup>24</sup>,  
12 J. Brunner<sup>41</sup>, M. Carson<sup>22</sup>, J. Casey<sup>5</sup>, M. Casier<sup>13</sup>, D. Chirkin<sup>27</sup>,  
13 A. Christov<sup>21</sup>, B. Christy<sup>16</sup>, K. Clark<sup>38</sup>, F. Clevermann<sup>19</sup>, S. Coenders<sup>1</sup>,  
14 S. Cohen<sup>24</sup>, D. F. Cowen<sup>38,37</sup>, A. H. Cruz Silva<sup>41</sup>, M. Danninger<sup>34</sup>,  
15 J. Daughhetee<sup>5</sup>, J. C. Davis<sup>17</sup>, C. De Clercq<sup>13</sup>, S. De Ridder<sup>22</sup>, P. Desiati<sup>27</sup>,  
16 M. de With<sup>9</sup>, T. DeYoung<sup>38</sup>, J. C. Díaz-Vélez<sup>27</sup>, M. Dunkman<sup>38</sup>, R. Eagan<sup>38</sup>,  
17 B. Eberhardt<sup>28</sup>, J. Eisch<sup>27</sup>, R. W. Ellsworth<sup>16</sup>, S. Euler<sup>1</sup>, P. A. Evenson<sup>31</sup>,  
18 O. Fadiran<sup>27</sup>, A. R. Fazely<sup>6</sup>, A. Fedynitch<sup>10</sup>, J. Feintzeig<sup>27</sup>, T. Feusels<sup>22</sup>,  
19 K. Filimonov<sup>7</sup>, C. Finley<sup>34</sup>, T. Fischer-Wasels<sup>40</sup>, S. Flis<sup>34</sup>, A. Franckowiak<sup>11</sup>,  
20 R. Franke<sup>41</sup>, K. Frantzen<sup>19</sup>, T. Fuchs<sup>19</sup>, T. K. Gaisser<sup>31</sup>, J. Gallagher<sup>26</sup>,  
21 L. Gerhardt<sup>8,7</sup>, L. Gladstone<sup>27</sup>, T. Glüsenkamp<sup>41</sup>, A. Goldschmidt<sup>8</sup>,  
22 G. Golup<sup>13</sup>, J. A. Goodman<sup>16</sup>, D. Góra<sup>41</sup>, D. Grant<sup>20</sup>, A. Groß<sup>30</sup>,  
23 M. Gurtner<sup>40</sup>, C. Ha<sup>8,7</sup>, A. Haj Ismail<sup>22</sup>, P. Hallen<sup>1</sup>, A. Hallgren<sup>39</sup>,  
24 F. Halzen<sup>27</sup>, K. Hanson<sup>12</sup>, D. Heereman<sup>42</sup>, P. Heimann<sup>1</sup>, D. Heinen<sup>1</sup>,  
25 K. Helbing<sup>40</sup>, R. Hellauer<sup>16</sup>, S. Hickford<sup>15</sup>, G. C. Hill<sup>2</sup>, K. D. Hoffman<sup>16</sup>,  
26 R. Hoffmann<sup>40</sup>, A. Homeier<sup>11</sup>, K. Hoshina<sup>27</sup>, W. Huelsnitz<sup>16,2</sup>, P. O. Hulth<sup>34</sup>,  
27 K. Hultqvist<sup>34</sup>, S. Hussain<sup>31</sup>, A. Ishihara<sup>14</sup>, E. Jacobi<sup>41</sup>, J. Jacobsen<sup>27</sup>,  
28 K. Jagielski<sup>1</sup>, G. S. Japaridze<sup>4</sup>, K. Jero<sup>27</sup>, O. Jlelati<sup>22</sup>, B. Kaminsky<sup>41</sup>,  
29 A. Kappes<sup>9</sup>, T. Karg<sup>41</sup>, A. Karle<sup>27</sup>, J. L. Kelley<sup>27</sup>, J. Kiryluk<sup>35</sup>, F. Kislak<sup>41</sup>,  
30 J. Kläs<sup>40</sup>, S. R. Klein<sup>8,7</sup>, J.-H. Köhne<sup>19</sup>, G. Kohnen<sup>29</sup>, H. Kolanoski<sup>9</sup>,  
31 L. Köpke<sup>28</sup>, C. Kopper<sup>27</sup>, S. Kopper<sup>40</sup>, D. J. Koskinen<sup>38</sup>, M. Kowalski<sup>11</sup>,  
32 M. Krasberg<sup>27</sup>, K. Krings<sup>1</sup>, G. Kroll<sup>28</sup>, J. Kunnen<sup>13</sup>, N. Kurahashi<sup>27</sup>,  
33 T. Kuwabara<sup>31</sup>, M. Labare<sup>13</sup>, H. Landsman<sup>27</sup>, M. J. Larson<sup>36</sup>,  
34 M. Lesiak-Bzdak<sup>35</sup>, M. Leuermann<sup>1</sup>, J. Leute<sup>30</sup>, J. Lünemann<sup>28</sup>, J. Madsen<sup>33</sup>,  
35 R. Maruyama<sup>27</sup>, K. Mase<sup>14</sup>, H. S. Matis<sup>8</sup>, F. McNally<sup>27</sup>, K. Meagher<sup>16</sup>,

\*Corresponding author. Email: wellons@icecube.wisc.edu, Phone: 304-542-4464, Address: Wisconsin Institutes for Discovery, 330 N. Orchard St., Madison, WI 53715

<sup>1</sup>Physics Department, South Dakota School of Mines and Technology, Rapid City, SD 57701, USA

<sup>2</sup>Los Alamos National Laboratory, Los Alamos, NM 87545, USA

<sup>3</sup>also Sezione INFN, Dipartimento di Fisica, I-70126, Bari, Italy

<sup>4</sup>Department of Physics, Sungkyunkwan University, Suwon 440-746, Korea

<sup>5</sup>NASA Goddard Space Flight Center, Greenbelt, MD 20771, USA

36 M. Merck<sup>27</sup>, P. Mészáros<sup>37,38</sup>, T. Meures<sup>12</sup>, S. Miarecki<sup>8,7</sup>, E. Middell<sup>41</sup>,  
 37 N. Milke<sup>19</sup>, J. Miller<sup>13</sup>, L. Mohrmann<sup>41</sup>, T. Montaruli<sup>21,3</sup>, R. Morse<sup>27</sup>,  
 38 R. Nahnhauser<sup>41</sup>, U. Naumann<sup>40</sup>, H. Niederhausen<sup>35</sup>, S. C. Nowicki<sup>20</sup>,  
 39 D. R. Nygren<sup>8</sup>, A. Obertacke<sup>40</sup>, S. Odrowski<sup>30</sup>, A. Olivas<sup>16</sup>, M. Olivo<sup>10</sup>,  
 40 A. O’Murchadha<sup>12</sup>, L. Paul<sup>1</sup>, J. A. Pepper<sup>36</sup>, C. Pérez de los Heros<sup>39</sup>,  
 41 C. Pfindner<sup>17</sup>, D. Pieloth<sup>19</sup>, N. Pirk<sup>41</sup>, J. Posselt<sup>40</sup>, P. B. Price<sup>7</sup>,  
 42 G. T. Przybylski<sup>8</sup>, L. Rädcl<sup>1</sup>, K. Rawlins<sup>3</sup>, P. Redl<sup>16</sup>, R. Reimann<sup>1</sup>,  
 43 E. Resconi<sup>30</sup>, W. Rhode<sup>19</sup>, M. Ribordy<sup>24</sup>, M. Richman<sup>16</sup>, B. Riedel<sup>27</sup>,  
 44 J. P. Rodrigues<sup>27</sup>, C. Rott<sup>17</sup>, T. Ruhe<sup>19</sup>, B. Ruzybayev<sup>31</sup>, D. Ryckbosch<sup>22</sup>,  
 45 S. M. Saba<sup>10</sup>, T. Salameh<sup>38</sup>, H.-G. Sander<sup>28</sup>, M. Santander<sup>27</sup>, S. Sarkar<sup>32</sup>,  
 46 K. Schatto<sup>28</sup>, M. Scheel<sup>1</sup>, F. Scheriau<sup>19</sup>, T. Schmidt<sup>16</sup>, M. Schmitz<sup>19</sup>,  
 47 S. Schoenen<sup>1</sup>, S. Schöneberg<sup>10</sup>, L. Schönherr<sup>1</sup>, A. Schönwald<sup>41</sup>, A. Schukraft<sup>1</sup>,  
 48 L. Schulte<sup>11</sup>, O. Schulz<sup>30</sup>, D. Seckel<sup>31</sup>, S. H. Seo<sup>34</sup>, Y. Sestayo<sup>30</sup>,  
 49 S. Seunarine<sup>33</sup>, C. Sheremata<sup>20</sup>, M. W. E. Smith<sup>38</sup>, M. Soiron<sup>1</sup>, D. Soldin<sup>40</sup>,  
 50 G. M. Spiczak<sup>33</sup>, C. Spiering<sup>41</sup>, M. Stamatikos<sup>17,5</sup>, T. Stanev<sup>31</sup>, A. Stasik<sup>41</sup>,  
 51 T. Stezelberger<sup>8</sup>, R. G. Stokstad<sup>8</sup>, A. Stöbl<sup>41</sup>, E. A. Strahler<sup>13</sup>, R. Ström<sup>39</sup>,  
 52 G. W. Sullivan<sup>16</sup>, H. Taavola<sup>39</sup>, I. Taboada<sup>5</sup>, A. Tamburro<sup>31</sup>,  
 53 S. Ter-Antonyan<sup>6</sup>, S. Tilav<sup>31</sup>, P. A. Toale<sup>36</sup>, S. Toscano<sup>27</sup>, M. Usner<sup>11</sup>,  
 54 D. van der Drift<sup>8,7</sup>, N. van Eijndhoven<sup>13</sup>, A. Van Overloop<sup>22</sup>, J. van Santen<sup>27</sup>,  
 55 M. Vehringer<sup>1</sup>, M. Voge<sup>11</sup>, M. Vraeghe<sup>22</sup>, C. Walck<sup>34</sup>, T. Waldenmaier<sup>9</sup>,  
 56 M. Wallraff<sup>1</sup>, R. Wasserman<sup>38</sup>, Ch. Weaver<sup>27</sup>, M. Wellons<sup>27,\*</sup>, C. Wendt<sup>27</sup>,  
 57 S. Westerhoff<sup>27</sup>, N. Whitehorn<sup>27</sup>, K. Wiebe<sup>28</sup>, C. H. Wiebusch<sup>1</sup>,  
 58 D. R. Williams<sup>36</sup>, H. Wissing<sup>16</sup>, M. Wolf<sup>34</sup>, T. R. Wood<sup>20</sup>, K. Woschnagg<sup>7</sup>,  
 59 C. Xu<sup>31</sup>, D. L. Xu<sup>36</sup>, X. W. Xu<sup>6</sup>, J. P. Yanez<sup>41</sup>, G. Yodh<sup>23</sup>, S. Yoshida<sup>14</sup>,  
 60 P. Zarzhitsky<sup>36</sup>, J. Ziemann<sup>19</sup>, S. Zierke<sup>1</sup>, A. Zilles<sup>1</sup>, M. Zoll<sup>34</sup>, B. Recht<sup>42</sup>,  
 61 C. Ré<sup>42</sup>

62 <sup>1</sup>III. Physikalisches Institut, RWTH Aachen University, D-52056 Aachen, Germany

63 <sup>2</sup>School of Chemistry & Physics, University of Adelaide, Adelaide SA, 5005 Australia

64 <sup>3</sup>Dept. of Physics and Astronomy, University of Alaska Anchorage, 3211 Providence Dr.,  
 65 Anchorage, AK 99508, USA

66 <sup>4</sup>CTSPS, Clark-Atlanta University, Atlanta, GA 30314, USA

67 <sup>5</sup>School of Physics and Center for Relativistic Astrophysics, Georgia Institute of  
 68 Technology, Atlanta, GA 30332, USA

69 <sup>6</sup>Dept. of Physics, Southern University, Baton Rouge, LA 70813, USA

70 <sup>7</sup>Dept. of Physics, University of California, Berkeley, CA 94720, USA

71 <sup>8</sup>Lawrence Berkeley National Laboratory, Berkeley, CA 94720, USA

72 <sup>9</sup>Institut für Physik, Humboldt-Universität zu Berlin, D-12489 Berlin, Germany

73 <sup>10</sup>Fakultät für Physik & Astronomie, Ruhr-Universität Bochum, D-44780 Bochum,  
 74 Germany

75 <sup>11</sup>Physikalisches Institut, Universität Bonn, Nussallee 12, D-53115 Bonn, Germany

76 <sup>12</sup>Université Libre de Bruxelles, Science Faculty CP230, B-1050 Brussels, Belgium

77 <sup>13</sup>Vrije Universiteit Brussel, Dienst ELEM, B-1050 Brussels, Belgium

78 <sup>14</sup>Dept. of Physics, Chiba University, Chiba 263-8522, Japan

79 <sup>15</sup>Dept. of Physics and Astronomy, University of Canterbury, Private Bag 4800,  
 80 Christchurch, New Zealand

81 <sup>16</sup>Dept. of Physics, University of Maryland, College Park, MD 20742, USA

82 <sup>17</sup>Dept. of Physics and Center for Cosmology and Astro-Particle Physics, Ohio State  
 83 University, Columbus, OH 43210, USA

84 <sup>18</sup>Dept. of Astronomy, Ohio State University, Columbus, OH 43210, USA

85 <sup>19</sup>Dept. of Physics, TU Dortmund University, D-44221 Dortmund, Germany

- 86 <sup>20</sup>Dept. of Physics, University of Alberta, Edmonton, Alberta, Canada T6G 2E1  
87 <sup>21</sup>Département de physique nucléaire et corpusculaire, Université de Genève, CH-1211  
88 Genève, Switzerland  
89 <sup>22</sup>Dept. of Physics and Astronomy, University of Gent, B-9000 Gent, Belgium  
90 <sup>23</sup>Dept. of Physics and Astronomy, University of California, Irvine, CA 92697, USA  
91 <sup>24</sup>Laboratory for High Energy Physics, École Polytechnique Fédérale, CH-1015 Lausanne,  
92 Switzerland  
93 <sup>25</sup>Dept. of Physics and Astronomy, University of Kansas, Lawrence, KS 66045, USA  
94 <sup>26</sup>Dept. of Astronomy, University of Wisconsin, Madison, WI 53706, USA  
95 <sup>27</sup>Dept. of Physics and Wisconsin IceCube Particle Astrophysics Center, University of  
96 Wisconsin, Madison, WI 53706, USA  
97 <sup>28</sup>Institute of Physics, University of Mainz, Staudinger Weg 7, D-55099 Mainz, Germany  
98 <sup>29</sup>Université de Mons, 7000 Mons, Belgium  
99 <sup>30</sup>T.U. Munich, D-85748 Garching, Germany  
100 <sup>31</sup>Bartol Research Institute and Department of Physics and Astronomy, University of  
101 Delaware, Newark, DE 19716, USA  
102 <sup>32</sup>Dept. of Physics, University of Oxford, 1 Keble Road, Oxford OX1 3NP, UK  
103 <sup>33</sup>Dept. of Physics, University of Wisconsin, River Falls, WI 54022, USA  
104 <sup>34</sup>Oskar Klein Centre and Dept. of Physics, Stockholm University, SE-10691 Stockholm,  
105 Sweden  
106 <sup>35</sup>Department of Physics and Astronomy, Stony Brook University, Stony Brook, NY  
107 11794-3800, USA  
108 <sup>36</sup>Dept. of Physics and Astronomy, University of Alabama, Tuscaloosa, AL 35487, USA  
109 <sup>37</sup>Dept. of Astronomy and Astrophysics, Pennsylvania State University, University Park,  
110 PA 16802, USA  
111 <sup>38</sup>Dept. of Physics, Pennsylvania State University, University Park, PA 16802, USA  
112 <sup>39</sup>Dept. of Physics and Astronomy, Uppsala University, Box 516, S-75120 Uppsala, Sweden  
113 <sup>40</sup>Dept. of Physics, University of Wuppertal, D-42119 Wuppertal, Germany  
114 <sup>41</sup>DESY, D-15735 Zeuthen, Germany  
115 <sup>42</sup>Dept. of Computer Sciences, University of Wisconsin, Madison, WI 53706, USA

---

116 **Abstract**

117 The IceCube project has transformed one cubic kilometer of deep natural  
118 Antarctic ice into a Cherenkov detector. Muon neutrinos are detected and their  
119 direction inferred by mapping the light produced by the secondary muon track  
120 inside the volume instrumented with photomultipliers. Reconstructing of the  
121 muon track from the observed light is challenging due to noise, light scattering  
122 in the ice medium, and the possibility of simultaneously having multiple muons  
123 inside the detector resulting from the large flux of cosmic ray muons.

124 This manuscript describes work on two problems: (1) the *track reconstruction*  
125 *problem*, in which, given a set of observations, the goal is to recover the  
126 track of a muon, and (2) the *coincident event problem*, which is to determine  
127 how many muons are active in the detector during a time window. Rather than  
128 solving these problems by developing more complex physical models that are  
129 applied at later stages of the analysis, our approach is to augment the detector's  
130 early reconstruction with data filters and robust statistical techniques. These  
131 can be implemented at the level of on-line reconstruction and therefore improve  
132 all subsequent reconstructions. Using the metric of median angular resolution, a

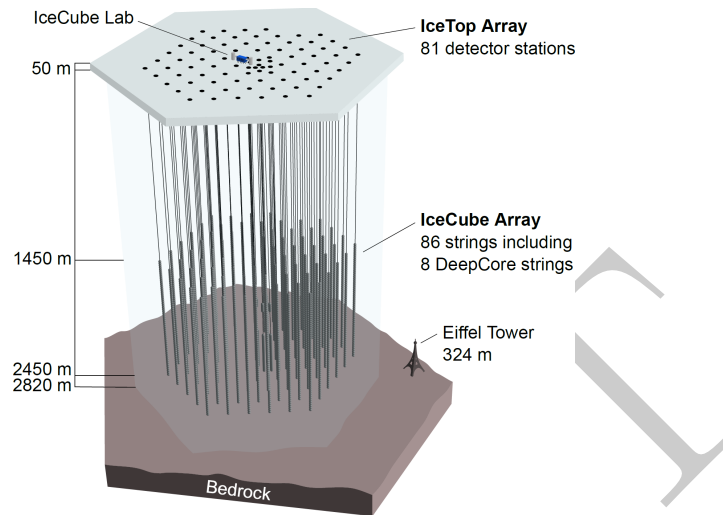


Figure 1: The IceCube neutrino detector in the Antarctic ice. A picture of the Eiffel Tower is shown for scale.

133 standard metric for track reconstruction, we improve the accuracy in the initial  
 134 reconstruction direction by 13%. We also present improvements in measuring  
 135 the number of muons in coincident events: we can accurately determine the  
 136 number of muons 98% of the time, which is an improvement of 86% over the  
 137 software previously used in IceCube.

138 *Keywords:* IceCube, Track reconstruction, Neutrino telescope, Neutrino  
 139 astrophysics, Robust Statistics

---

140 **1. Introduction**

141 The IceCube neutrino detector searches for neutrinos that are generated by  
 142 the universe’s most violent astrophysical events: exploding stars, gamma ray  
 143 bursts, and cataclysmic phenomena involving black holes and neutron stars [1].  
 144 The detector, roughly one cubic kilometer in size, is located near the geographic  
 145 South Pole and is buried to a depth of about 2.5 km in the Antarctic ice [2].  
 146 The detector is illustrated in Figure 1 and a more complete description is given  
 147 in Section 2.

148 When a neutrino enters the telescope, it occasionally interacts in the ice and  
 149 generates a muon. The neutrino direction can be inferred from a reconstruction  
 150 of the muon track. Muons are also generated by cosmic rays interacting  
 151 in the atmosphere, and separation of the background of cosmic ray muons and  
 152 neutrino-induced muons is a necessary step for neutrino analysis. This separation  
 153 is challenging, as the number of observed cosmic ray muons exceeds the

154 number of observed neutrino muons by over five orders of magnitude [3].

155 The primary mechanism for separating the cosmic ray muons from the neu-  
156 trino muons is reconstructing the muon track and determining whether the  
157 muon was traveling downwards into the Earth or upwards out of the Earth.  
158 Since neutrinos can penetrate through the Earth but cosmic ray muons cannot,  
159 it follows that a muon traveling out of the Earth must have been generated by a  
160 neutrino. Thus, by selecting only the muons that are reconstructed as up-going,  
161 the cosmic ray muons can, in principle, be removed from the data. Since the  
162 number of cosmic ray muons overwhelms the number of neutrino muons, high  
163 accuracy is critical for preventing erroneous reconstruction of cosmic ray muons  
164 as neutrino-induced.

165 Here, we examine two problems that arise in the separation of cosmic ray  
166 muons from neutrino muons in the IceCube detector:

- 167 1. *Reconstruction*, in which the track of a muon is reconstructed from the  
168 observed light at different positions and times in the detector.
- 169 2. *Coincident Event Detection*, in which we detect the number of muons  
170 inside the detector, and assign observed photons to a muon.

171 Sophisticated reconstruction techniques have been developed that computa-  
172 tionally model in detail the muon's Cherenkov cone as well as the scattering  
173 and absorption of photons through layers of Antarctic ice with varying optical  
174 properties [3–5]. Rather than further refining these techniques, the current work  
175 focusses on improving the statistical techniques and optimizing data filtering in  
176 the early online track reconstruction performed on the data in real time at the  
177 South Pole. Besides benefiting directly any analysis that uses the online recon-  
178 struction such as the search for cosmogenic neutrinos, any later analysis will  
179 benefit from improvements made at the early stages of the data collection.

### 180 1.1. *Related Work*

181 Track reconstruction and coincident event detection challenges are ubiqui-  
182 tous in particle physics [6–8], both in particle accelerators and cosmic particle  
183 detectors. While the work described in this manuscript builds on the previous  
184 technique developed for the IceCube detector [3], these techniques are general  
185 purpose, and potentially have applications in detectors beyond IceCube.

### 186 1.2. *Outline*

187 We begin by describing the IceCube detector and track reconstruction chal-  
188 lenges in Section 2. In Section 3, we describe the reconstruction pipeline in-  
189 cluding the prior IceCube software, then we present improvements to the online  
190 tracking algorithm and discuss the results. Section 4 describes improvements  
191 on coincident event detection, and follows a parallel structure to Section 3. We  
192 conclude in Section 5.

## 193 2. IceCube Detector and Track Reconstruction Challenges

194 The IceCube detector is composed of 5,160 optical detectors, each containing  
195 a photomultiplier tube (PMT) and onboard digitizer [9]. The PMTs are spread  
196 over 86 vertical strings arranged in a hexagonal shape, with a total instrumented  
197 volume of approximately one cubic kilometer. The PMTs on a given string  
198 are separated vertically by 17 m, and the string-to-string separation is roughly  
199 125 m.

200 At an abstract level, the IceCube detector operates by detecting muons  
201 as they travel through the instrumented volume of ice. As the muon travels  
202 through the detector, it radiates light [4], which is observed by the PMTs and  
203 quantized into discrete *hits* [10]. The detector uses several trigger criteria. The  
204 most commonly used trigger selects time intervals where eight PMTs (with local  
205 coincidences) fired within 5 microseconds. When a trigger occurs, all data within  
206 a 10 microsecond trigger window is saved, becoming an *event*. If the number of  
207 hits in an event is sufficiently large, the muon track reconstruction algorithm is  
208 triggered.

209 There are several challenges for the reconstruction algorithms used in the  
210 detector. Varying optical properties of the ice affect reconstruction accuracy,  
211 the data may contain outlier hits due to uncorrelated noise, and there are finite  
212 computational resources available to tracking code run on-site.

213 *Modeling Difficulties.* The details of the ice's optical properties are nontrivial to  
214 model. Light propagating through the ice is affected by scattering and absorp-  
215 tion. These effects cannot be analytically calculated and the optical properties  
216 of the ice vary with depth [5].

217 *Noise.* The noise inherent in the data is another challenge. Noise hits can  
218 arise either from the thermal background of the photocathode, or from photons  
219 generated by radioactive decay inside the PMT [9].

220 *Computational Constraints.* The reconstruction algorithms are also limited in  
221 complexity by the computing resources available at the South Pole. The track  
222 reconstruction algorithm has to process about 3,000 muons per second, algo-  
223 rithms with excessive computational demands are discouraged.

## 224 3. Reconstruction Improvement

225 As shown in the following, augmenting the reconstruction algorithm with  
226 some basic filters and classical data analysis techniques results in significant  
227 improvement in the reconstruction algorithm's accuracy.

### 228 3.1. Prior IceCube Software

229 The muon track reconstruction process (outlined in Figure 2) starts when the  
230 number of detected hits exceeds a preset threshold and initiates data collection.

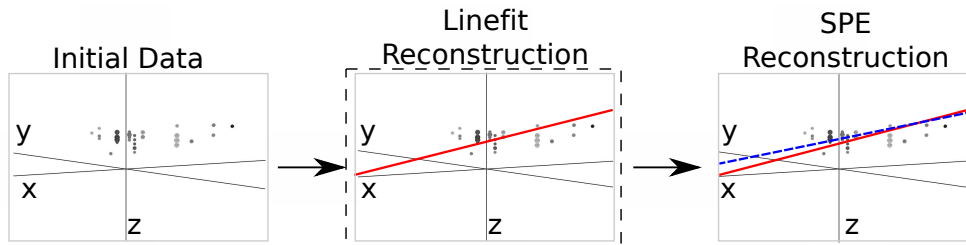


Figure 2: The reconstruction pipeline used to process data in the IceCube detector. After initial data are collected, it is then processed by some basic noise filters, which remove clear outliers. This cleaned data are processed by a basic reconstruction algorithm (solid line), which is used as the seed for the more sophisticated reconstruction algorithm (dashed line). The sophisticated reconstruction is then evaluated as a potential neutrino. The work presented in this manuscript makes changes to the basic reconstruction step (indicated by the dashed box).

231 After the initial data are collected, the event then passes through a series of  
 232 basic filters to remove obvious outliers [11].

233 This is followed by a basic reconstruction algorithm, *linefit* [12], that dis-  
 234 regards the Cherenkov cone and instead finds the track that minimizes the sum  
 235 of the squares of the distances between the track and the hits. More formally,  
 236 assume there are  $N$  hits; denote the position and time of the  $i$ th hit as  $\vec{x}_i$  and  $t_i$ ,  
 237 respectively. Let the reconstructed muon track have a velocity of  $\vec{v}$ , and let the  
 238 reconstructed track pass through point  $\vec{x}_0$  at time  $t_0$ . Then linefit reconstruction  
 239 solves the *least-squares* optimization problem

$$\min_{t_0, \vec{x}_0, \vec{v}} \sum_{i=1}^N \rho_i(t_0, \vec{x}_0, \vec{v})^2, \quad (1)$$

240 where

$$\rho_i(t_0, \vec{x}_0, \vec{v}) = \|\vec{v}(t_i - t_0) + \vec{x}_0 - \vec{x}_i\|_2. \quad (2)$$

241 Linefit is an approximation primarily used to generate an initial track or *seed*  
 242 for a more sophisticated reconstruction.

243 The reconstruction algorithm for the sophisticated reconstruction is *Single-*  
 244 *Photo-Electron-Fit (SPE fit)* [3]. SPE fit uses the least-squares reconstruction,  
 245 the event data, and a parameterized probability distribution function of scat-  
 246 tering in ice [3] to reconstruct the muon track. The SPE fit is the primary  
 247 reconstruction algorithm used in the initial data selection and filtering run at  
 248 the detector site, and the fit serves as a seed track to the more complex recon-  
 249 structions used in off-site data analyses.

### 250 3.2. Algorithm Improvement

251 If angular deviations of the initial seed are large ( $\approx 5$ -10 deg), the simple  
 252 subsequent reconstruction, SPE, often does not converge to the global minimum  
 253 and the efficiency is degraded. This can be resolved by more advanced but

254 time consuming reconstruction algorithms or by improving the initial seed as  
255 described here.

256 As indicated in Equation 1, a least-squares fit models the muon as a single  
257 point moving in a straight line, and hits are penalized quadratically in their  
258 distance from this line. Thus there is an implicit assumption in this model:  
259 that all the hits will be near the muon. This assumption has several pitfalls:

- 260 1. It doesn't account for the distinct Cherenkov emission profile neither from  
261 the muon itself, nor from charged particles in showers initiated by stochastic  
262 energy losses of the muon along its track.
- 263 2. It ignores the scattering effects of the ice medium. Some of the photons can  
264 scatter for over a microsecond, which means that when they are recorded  
265 by a PMT, the muon will be over 300 m away.
- 266 3. While the noise reduction steps remove most of the outlier noise, the noise  
267 hits that survive can be far from the muon. Since these outliers are given  
268 quadratic weight, they exert a huge influence over the model.

269 The first two pitfall occurs because the model is incomplete and does not  
270 accurately model the data, and the third demonstrates that the model is not  
271 robust to noise. The solution to this is twofold: improve the model and increase  
272 the noise robustness by replacing least squares with robust statistical techniques.

### 273 3.2.1. Improving the Model

274 While disregarding the Cherenkov profile is inherent to the simplified model  
275 chosen for speed reasons, removing hits generated by photons that scattered  
276 for a significant length of time will mitigate the effect of ignoring the photon  
277 scattering in the ice. We found that a basic filter could identify these scattered  
278 hits, and improve accuracy by of almost a factor of two by removing them from  
279 the dataset.

280 More formally, for each hit  $h_i$ , the algorithm looks at all neighboring hits  
281 within a neighborhood of  $r$ , and if there exists a neighboring hit  $h_j$  with a time  
282 stamp that is  $t$  earlier than  $h_i$ , then  $h_i$  is considered a scattered hit, and is  
283 not used in the basic reconstruction algorithm. Optimal values of  $r$  and  $t$  were  
284 found to be 156 m and 778 ns by tuning them on simulated muon data with an  
285  $E^{-2}$  power law spectrum.

### 286 3.2.2. Adding Robustness to Noise

287 As described in equation 1, the least squares model gives outliers quadratic  
288 weight, whereas we would prefer that outliers had zero weight. There are robust  
289 models in classical statistics designed to marginalize outliers. We determined  
290 that replacing the least-squares model with a Huber fit [13] improves the recon-  
291 struction accuracy.

292 More formally, we replace Equation 1 with the optimization problem:

$$\min_{t_0, \vec{x}_0, \vec{v}} \sum_{i=1}^N \phi(\rho_i(t_0, \vec{x}_0, \vec{v})), \quad (3)$$



Table 1: Median angular resolution (degrees) for reconstruction improvements. The first line is the accuracy of the prior least-squares model, and the subsequent lines are the accuracy measurements from cumulatively adding improvements into the basic reconstruction algorithm.

Algorithm	$\theta_{med}$
Linefit Reconstruction (Least-Squares)	9.917
With Addition of Logical Filter	5.205
With Addition of Huber Regression	4.672
With Addition of Outlier Removal	4.211

293 where the Huber penalty function  $\phi(\rho)$  is defined as

$$\phi(\rho) \equiv \begin{cases} \rho^2 & \text{if } \rho < \mu \\ \mu(2\rho - \mu) & \text{if } \rho \geq \mu \end{cases} \quad (4)$$

294 Here,  $\rho_i(t_0, \vec{x}, \vec{v})$  is defined in Equation 2 and  $\mu$  is a constant calibrated to the  
 295 data (on simulated muon events with an  $E^{-2}$  power law spectrum, the optimal  
 296 value of  $\mu$  is 153 m).

297 The Huber penalty function has two regimes. In the near-hit regime ( $\rho < \mu$ ),  
 298 hits are assumed to be strongly correlated with the muon’s track, and the Huber  
 299 penalty function behaves like least squares, giving these hits quadratic weight.  
 300 In the far-hit regime ( $\rho \geq \mu$ ), hits are given linear weights as they are more  
 301 likely to be noise.

302 In addition to its attractive robustness properties, the Huber fit’s weight  
 303 assignment also has the added benefit that it inherently labels points as outliers  
 304 (those with  $\rho \geq \mu$ ). Thus, once the Huber fit is computed, we can go one step  
 305 farther and simply remove the labeled outliers from the dataset. A better fit is  
 306 then obtained by computing the least-squares fit on the data with the outliers  
 307 removed. The entire algorithm has a mean runtime that is approximately six  
 308 times longer than Linefit’s mean runtime.

### 309 3.3. Results

310 The goal is to improve the accuracy of the reconstruction in order to better  
 311 separate neutrinos from cosmic rays. Thus we present three measurements: (1)  
 312 the accuracy change between linefit and the new algorithm, (2) the accuracy  
 313 change when SPE is seeded with the new algorithm instead of linefit, and (3)  
 314 the improvement in separation between neutrinos and cosmic rays.

315 To measure the improvement generated by the changes, we use the metric of  
 316 *median angular resolution*  $\theta_{med}$ , which is a standard metric within the collab-  
 317 oration. The angular resolution of a reconstruction is the arc-distance between  
 318 the reconstruction and the true track. The dataset is drawn from simulated  
 319 neutrino data designed to be similar to that observed by the detector.

320 We can improve the median angular resolution of the basic reconstruction  
 321 by 57.6%, as shown in Table 1. Seeding SPE with the improved basic recon-  
 322 struction generates an improvement in the angular resolution of 12.9%. These

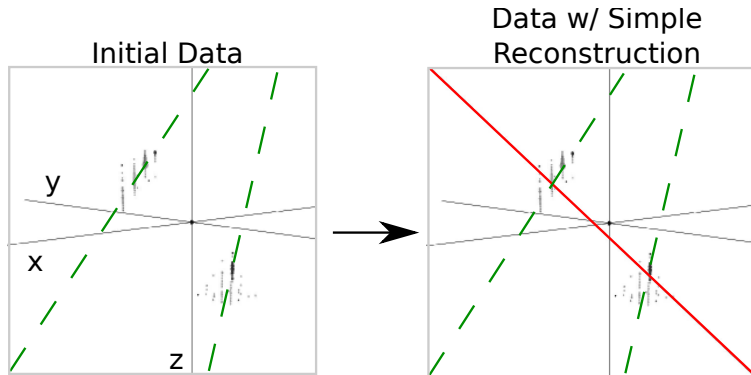


Figure 3: In this example, an event that is clearly composed of two muons (actual tracks shown as dashed lines) is treated as a single muon, and thus the reconstruction (solid line) is inaccurate.

323 improvements in the reconstruction algorithm result in 10% fewer atmospheric  
 324 muons erroneously reconstructed as up-going, and 1% more muons correctly  
 325 reconstructed as up-going.

#### 326 4. Coincident Event Improvements

327 In the second study, we look at the problem of determining when more than  
 328 one muon has entered the detector. In the most common case, a single muon  
 329 will pass through the detector and generate an event before exiting. These events  
 330 are processed by the pipeline described in Figure 2. However, for roughly 9%  
 331 of the events collected by the data collection algorithm, more than one muon  
 332 will be passing through the detector simultaneously, an occurrence known as a  
 333 *coincident event*.

334 One of the primary sources of background noise in IceCube analyses is coinci-  
 335 dent background muons that have been erroneously reconstructed as neutrinos.  
 336 To see why this occurs, consider the coincident event shown in Figure 3. There  
 337 are two clear groups of hits; however, the reconstruction algorithm treats them  
 338 as a single group, resulting in an erroneous reconstruction. In the ideal case, the  
 339 reconstruction algorithm would identify coincident events and split them, as in  
 340 Figure 4.

341 The challenge in this example is determining the number of muons in an  
 342 event. Our studies show that a simple spatial clustering algorithm can solve  
 343 this classification problem with less than 2% error.

##### 344 4.1. Prior IceCube Software

345 Coincident events have been a concern in the IceCube analysis [14] for years,  
 346 and some software has been developed to handle coincident events. As a baseline  
 347 of comparison, we use the *TTrigger* software, which is described in [15].

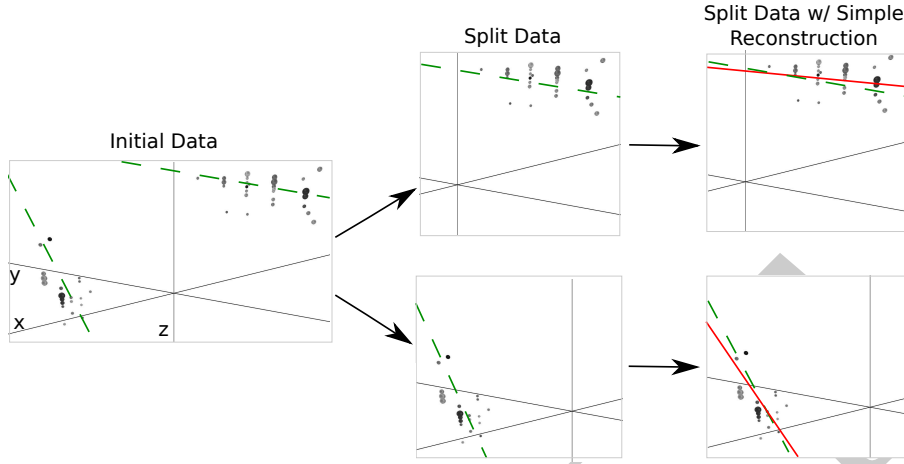


Figure 4: Ideally, the detector would split coincident events before computing the reconstruction. Splitting the event results in more accurate reconstructions (reconstructions shown as solid lines, true muon tracks shown as dashed lines). Note the difference in the reconstructions compared with Figure 3.

#### 348 4.2. Algorithm Improvement

349 Here we present a proximal clustering algorithm. The intuition in proximal  
 350 clustering is that points local in space and time are probably from the same  
 351 muon. The proximal clustering algorithm iterates through each pair of hits  
 352  $(i, j)$  and builds an adjacency matrix  $\mathbf{A}$  as

$$\mathbf{A}_{ij} = \begin{cases} 1 & \text{if } \|\Delta x^2 + \Delta y^2 + \Delta z^2 + (c\Delta t)^2\|_2 \leq \alpha, \\ 0 & \text{otherwise} \end{cases} \quad (5)$$

353 where  $\Delta x, \Delta y, \Delta z$  and  $\Delta t$  are the space and time differences between the pair  
 354 of hits, and  $\alpha$  is tuned to the data (in this application, the optimal value of  
 355  $\alpha$  is 450 m). The clustering can be recovered by extracting the connected  
 356 components of the graph defined by  $\mathbf{A}$ . A connected component of a graph is a  
 357 subgraph such that there exist a path between any two vertices of this subgraph.

##### 358 4.2.1. Improving the Model

359 When implemented naively, proximal clustering succeeded for the majority  
 360 of the events, but failed if there was a gap in the muon track, which can occur  
 361 when the muon travels through dusty ice layers with short scattering length. If  
 362 there is a significantly large gap, the algorithm erroneously separates the hits  
 363 into two clusters.

364 To compensate, an additional heuristic is added, *track connecting*. After the  
 365 data segmentation is finished, track connecting determines if separate clusters  
 366 should be combined. It computes the mean position and time of each cluster,  
 367 and connects a hypothetical muon track  $T$  between each pair of subspaces.

368 It checks if the speed  $s$  of the hypothetical track is within 25% of the speed  
 369 of light  $c$ , and it checks that the mean distance between hits and  $T$  in both  
 370 clusters is less than 60 m. If  $T$  passes both checks, the clusters are combined.

#### 371 4.2.2. Adding Robustness to Noise

372 Proximal clustering is susceptible to noise. Noise hits close to two disjoint  
 373 tracks will be considered adjacent to both tracks, and thus can connect the two  
 374 tracks in the adjacency matrix.

375 One heuristic that worked well at mitigating this problem was to not use  
 376 all the hits in building the adjacency matrix. During data collection, some hits  
 377 are flagged as having a *local coincidence condition*, which indicates that both  
 378 they and a neighboring PMT reported a hit. These hits have a high probability  
 379 of not being noise hits, and thus exclusively using them to build the adjacency  
 380 matrix mitigates the problem of erroneously connecting two tracks.

381 After the proximal clustering algorithm has extracted the tracks from the  
 382 adjacency matrix, the hits not used in the construction of the adjacency matrix  
 383 are simply assigned to the closest reconstructed track.

### 384 4.3. Results

385 There were two competing goals for coincident event detection algorithms:  
 386 the algorithm should be conservative enough that events containing single tracks  
 387 are not erroneously split, and aggressive enough that a useful fraction of coin-  
 388 cident events are split correctly. Our algorithm is tuned to keep almost all  
 389 of the single events correctly unsplit, while still correctly splitting 80% of the  
 390 coincident events.

#### 391 4.3.1. Measurements

392 We modified the reconstruction pipeline shown in Figure 2, in between the  
 393 noise cleaning and the basic reconstruction, by adding a step for coincident event  
 394 detection, as shown in Figure 4. This step takes cleaned data and attempts to  
 395 classify the event as a single-track or multiple-track event.

396 We ran each algorithm on two datasets of simulated data. One dataset  
 397 comprised single-muon events, and the other dataset comprised multiple-muon  
 398 events. In each dataset, we measured the classification error  $E$ , which is the  
 399 fraction of events that were misclassified. To get a global measurement, we  
 400 compute the *total error*  $E_{tot}$ , defined as

$$E_{tot} = w_{\text{Single}}E_{\text{Single}} + w_{\text{Multiple}}E_{\text{Multiple}}. \quad (6)$$

401 For computing  $E_{tot}$ , we use  $w_{\text{Single}} = 0.917$  and  $w_{\text{Multiple}} = 0.083$ , which is  
 402 the frequency in which single-muon and multiple-muon events appear in data  
 403 simulating the distribution of events that trigger the reconstruction algorithm.

404 We present the results for the coincident event problem by measuring how  
 405 well each algorithm performs at determining the number of subspaces in an  
 406 event.

Table 2: Error Rates for Classification Algorithms

Algorithm	$E_{\text{Single}}\%$	$E_{\text{Multiple}}\%$	$E_{\text{tot}}\%$
Trivial	0.0	100.0	8.3
TTrigger	11.5	31.8	13.2
Proximal clustering	0.2	18.9	1.8

407 There are two natural comparisons for the work: the prior software TTrigger,  
 408 as well as the trivial algorithm, which always classifies each event as a single-  
 409 track event. Clearly, the latter will always get the single-track events correct,  
 410 and always get the multiple-track events wrong. We provide a comparison of  
 411 these techniques in Table 2. As shown, the new algorithm classifies the number  
 412 of muons in the detector 86% better than TTrigger.

## 413 5. Conclusions

414 We found that significant improvements can be achieved in the IceCube’s on-  
 415 line track reconstruction by employing some classical data analysis algorithms.  
 416 Optimizing data filtering and refining the least-square model have led to signif-  
 417 icant improvements in the accuracy of the reconstruction direction. The new  
 418 reconstruction software is fast enough to run on-site, and is now included in all  
 419 IceCube analyses.

420 We also looked at the problem of determining the number of muons in the  
 421 detector. We found that proximal clustering with some basic heuristics could  
 422 correctly determine whether an event contained a single muon or multiple muons  
 423 with less than 2% error, yielding an 86% improvement over the prior software.

## 424 References

- 425 [1] IceCube Collaboration, IceCube webpage, <http://icecube.wisc.edu/>.
- 426 [2] IceCube Collaboration, First year performance of the IceCube neutrino  
 427 telescope, *Astroparticle Physics* 26 (3) (2006) 155–173.
- 428 [3] IceCube Collaboration, Muon track reconstruction and data selection tech-  
 429 niques in AMANDA, *Nuclear Instruments and Methods in Physics Re-*  
 430 *search Section A* 524 (2004) 169–194.
- 431 [4] IceCube Collaboration, Measurement of South Pole ice transparency with  
 432 the IceCube LED calibration system IceCube Collaboration, *Nuclear In-*  
 433 *struments and Methods in Physics Research Section A* (2013) 73–89.
- 434 [5] The AMANDA Collaboration, Optical properties of deep glacial ice at the  
 435 south pole, *Journal of Geophysical Research* 111 (D13) (2006) D13203.

- 436 [6] ATLAS Collaboration, Tracking and vertexing with the ATLAS detector at  
437 the LHC, Nuclear Instruments and Methods in Physics Research Section A:  
438 Accelerators, Spectrometers, Detectors and Associated Equipment 650 (1)  
439 (2011) 218–223.
- 440 [7] R. S. Chivukulaa, M. Goldenaa, E. H. Simmons, Multi-jet physics at hadron  
441 colliders, Nuclear Physics B 363 (1) (1991) 83–96.
- 442 [8] S. Ellis, J. Huston, K. Hatakeyama, P. Loch, M. Tönnesmann, Jets in  
443 hadron–hadron collisions, Progress in Particle and Nuclear Physics (60)  
444 (2008) 484–551.
- 445 [9] IceCube Collaboration, Calibration and characterization of the IceCube  
446 photomultiplier tube, Nuclear Instruments and Methods in Physics Re-  
447 search Section A 618 (2010) 139–152.
- 448 [10] IceCube Collaboration, The icecube data acquisition system: Signal cap-  
449 ture, digitization, and timestamping, Nuclear Instruments and Methods in  
450 Physics Research Section A 601 (3) (2009) 294–316.
- 451 [11] M. Ackermann, Searches for signals from cosmic point-like sources of high  
452 energy neutrinos in 5 years of AMANDA-II data, Ph.D. thesis, Humboldt-  
453 Universität zu Berlin (2006).
- 454 [12] V. Stenger, Track fitting for DUMAND-II Octagon Array, Tech. rep., Uni-  
455 versity of Hawai’i at Manoa (1990).
- 456 [13] S. Boyd, L. Vandenberghe, Convex Optimization, Cambridge University  
457 Press, 2009.
- 458 [14] IceCube Collaboration, Measurement of the atmospheric neutrino energy  
459 spectrum from 100 GeV to 400 TeV with IceCube, Physical Review D  
460 83 (1).
- 461 [15] D. Chirkin, Measurement of the atmospheric neutrino energy spectrum  
462 with IceCube, Proceedings of the 31st ICRC.